agronomy

MDPI

Article

Study on the Influence Mechanism of Soil Covering and Compaction Process on Maize Sowing Uniformity Based on DEM–MBD Coupling

Kuo Sun [1], Chenglin He [1], Qing Zhou [2], Xinnan Yu [1], Qiu Dong [1], Wenjun Wang [1], Yulong Chen [1], Mingwei Li [1], Xiaomeng Xia [1], Yang Wang [3] and Long Zhou [1,*]

[1] School of Agricultural Engineering and Food Science, Shandong University of Technology, Zibo 255000, China
[2] Lutai School of Textile and Apparel, Shandong University of Technology, Zibo 255000, China
[3] School of Biological and Agricultural Engineering, Jilin University, Changchun 130022, China
* Correspondence: zhoulong18@mails.jlu.edu.cn; Tel.: +86-0533-2786398

Abstract: In the production process of maize, the uniformity of maize sowing is one of the main factors affecting maize yield. The effect of soil coverage and the compaction process on sowing uniformity, as the final link in determining the seed bed position, needs to be further investigated. In this paper, the parameters between soil particles and boundaries are calibrated using the Plackett–Burman test and the central composite design. Furthermore, based on the DEM–MBD coupling, the influence of soil coverage and the compaction process on the seed position of the seeding monomer at different forward speeds are analysed. It was found that the adhesion between the soil and the soil-touching component can have a significant effect on the contact process between the component and the soil. Therefore, the EEPA model was used to analyse the soil–component interaction process and the contact parameters between the soil and components were obtained for the calibration. Further, based on the above work, it was found that before and after mulching, the displacement of seed particles of all shapes in the longitudinal direction increased significantly with the increase in the advancement speed of the sowing unit, while the displacement of seed particles in the transverse and sowing depth directions decreased with the increase in the advancement speed of the unit. In addition, before and after suppression, as the forward speed of the sowing unit increased, the displacement of seed particles of all shapes in the longitudinal and transverse directions gradually increased, and the displacement of seed particles of all shapes in the direction of the sowing depth decreased; the disturbance of seed displacement by the mulch suppression process was not related to seed shape. As the operating speed of the seeding unit increased, the mulching compaction process significantly reduced the sowing uniformity of maize seeds. This paper provides a theoretical basis for the next step in optimising the structure and working process of the soil coverage and the compaction.

Keywords: corn sowing; covering with soil and suppression; DEM–MBD coupling; parameter calibration; sowing uniformity

Citation: Sun, K.; He, C.; Zhou, Q.; Yu, X.; Dong, Q.; Wang, W.; Chen, Y.; Li, M.; Xia, X.; Wang, Y.; et al. Study on the Influence Mechanism of Soil Covering and Compaction Process on Maize Sowing Uniformity Based on DEM–MBD Coupling. *Agronomy* **2024**, *14*, 2883. https://doi.org/10.3390/agronomy14122883

Academic Editors: Mavromatis Theodoros, Thomas Alexandridis and Vassilis Aschonitis

Received: 25 October 2024
Revised: 28 November 2024
Accepted: 2 December 2024
Published: 3 December 2024

1. Introduction

As one of the three principal food crops, the production of maize is intrinsically linked to the stability and development of society. In the production of maize, the uniformity of maize sowing is one of the main factors affecting maize yield. The primary causes of uneven sowing consist of the maize seeds' rebound upon contact with the soil upon discharge from the seeding apparatus and the disruption of seed placement during the covering with soil and suppression process. Diminished sowing uniformity reduces inter-plant spacing and leads to narrower row gaps among maize crops, compromising the field's microenvironment. This compromise adversely impacts the efficacy of light, thermal, and other resource utilization, ultimately curtailing maize yield potential [1]. Therefore,

exploring how to mitigate seed disturbance during covering with soil and suppression has become a central element in improving the quality of maize sowing operations.

During the sowing process, the displacement of seeds induced by the covering with soil and suppression operations constitutes the principal factor leading to non-uniform seed distribution. Wang et al. [2] meticulously investigate the influence exerted by each parameter of the figure-of-eight covering device on the displacement resulting from seed bouncing. They use a uniform design to construct a mathematical model of the covering device parameters, the machine forward speed, and the seed bouncing displacement, and finally obtain the optimal parameter combination. In a meticulous study by Wang et al. [3], the impacts of individual structural parameters of both the covering device and the furrower, alongside operational velocity, explore seed bounce displacement. The research further validates the analytical practicability by simulating the mulching and suppression processes by leveraging the Smooth Particle Dynamics (SPD) methodology. Nonetheless, it is challenging to precisely acquire data on the forces, displacements of particles, and velocities of particles between the seed particles and the mechanical components or the soil through experimental and smooth particle methods. These are crucial for the design and optimisation of the components of agricultural machinery, thereby limiting the investigation of the mechanism. As computer technology has advanced, employing the discrete element method (DEM) [4] to analyse the contact interactions between particles and mechanical components can address the aforementioned issues. Presently, the DEM has evolved into a widely used method for analysing the interactions of particles in contact with pertinent mechanical components and has been extensively applied in the field of agricultural engineering [5–9].

In the process of soil loosening, ditching, covering with soil, and suppression, some parts come into contact with the soil and produce contact effects. Some scholars do not consider the cohesive effect of the contact of mechanical parts with soil [10–15]. Other scholars studying the contact of mechanical parts with the soil consider the adhesive effect between the parts and the soil. Ucgul et al. [16] integrate the Hysteretic Spring contact model and Linear Cohesion contact model for contact action between soil particles as well as between soil particles and tillage components. They validate the models by a direct shear test and trenching test with furrowers. Barr et al. [17,18] analyse the performance of furrowers based on the integrated Hysteretic Spring contact model and Linear Cohesion contact model. Mak et al. [19] use a parallel bonding model to simulate the contact interaction between soil particles and the boundary and obtain the contact parameters between soil particles and the boundary through calibration tests. Therefore, for the contact between the soil and the component, whether it is necessary to consider the adhesion of the soil to the component needs to be further investigated.

After determining the mechanical model of the contact between the soil and the components, the next step is to simulate and analyse the effect of the soil coverage and the compaction process on the uniformity of seeding. The motion of the seeding unit is a complex motion process, and its working process needs to be studied with the help of the coupled DEM–MBD method. Xing et al. [20] established a coupled DEM–MBD simulation model of a potato planter and optimised the spoon chain potato seed measurement device. Fang et al. [21] used a DEM–MBD coupled multi-body dynamics approach to study the bionic elastic tooth-residual film–soil interaction perturbations. Xie et al. [22] established a coupled DEM–MBD simulation model of a seeding machine and determined the best combination of process parameters for optimal work performance. However, there are few reports on the study of the soil coverage and suppression process of the seeding unit using DEM–MBD coupling.

Based on the aforementioned issues, this paper statistically analyses the maximum adhesion force during normal contact between the soil and interacting components in the sown field. The objective is to explore how adhesion between the boundary and the soil affects the intercropping process. The parameters for interactions among soil particles, soil particles, and seed particles, and soil particles and the boundary are calibrated using the

Plackett–Burman test and the central composite design. By employing the discrete element method (DEM) coupled with multi-rigid body dynamics (MBD), the study simulates and analyses the influence of the mulch suppression process on the seed placement of the seeding monomer at different forward speeds. This provides a theoretical basis for further optimizing the soil covering and suppression processes.

2. Materials and Methods

2.1. Selection of Contact Models Among Soil and Soil Interaction Elements

In this section, by examining the normal interaction between the soil contact component (galvanised steel) and the soil, this article derives the contact force and displacement curves between the soil and the boundary to determine the maximum adhesion force. Subsequently, the pressure between the boundary and the soil is computed based on the contact area. By analysing these calculated pressures, the influence of the soil's adhesion to the boundary on the contact process can be assessed.

To prepare soil samples with 15%, 20%, and 25% moisture content, the amount of water to be added to prepare soil samples with 15%, 20%, and 25% moisture content is calculated according to the following formula, after first obtaining the moisture content of the soil samples by the atmospheric pressure constant temperature drying method.

$$m_1 = \frac{m_0}{1 + 0.01 w_0} \times 0.01(w_1 - w_0) \tag{1}$$

where m_1 is the amount of water added to a soil sample that needs to be formulated with a certain moisture content, g; m_0 is the mass of the soil sample before treatment, g; w_0 is the moisture content of the soil sample before treatment, %; and w_1 is the moisture content of the soil sample to be formulated, %.

In this paper, the power sensing element accuracy is 0.0001 g with an error of less than 0.001% using the TA.XTC-18 texture analyser (Bosin, Shanghai, China). The diagrammatic representation of the device is illustrated in Figure 1. The test steps were as follows: First, adjust the texture analyser to a suitable height and place a soil sample directly under the probe. Then, the texture analyser probe moves downward at a speed of 1 mm/s until the probe causes a 30% change in the height of the soil, at which point the probe moves upwards. Finally, the curves and data for force versus displacement are obtained. Three replicate tests are performed for each set of conditions.

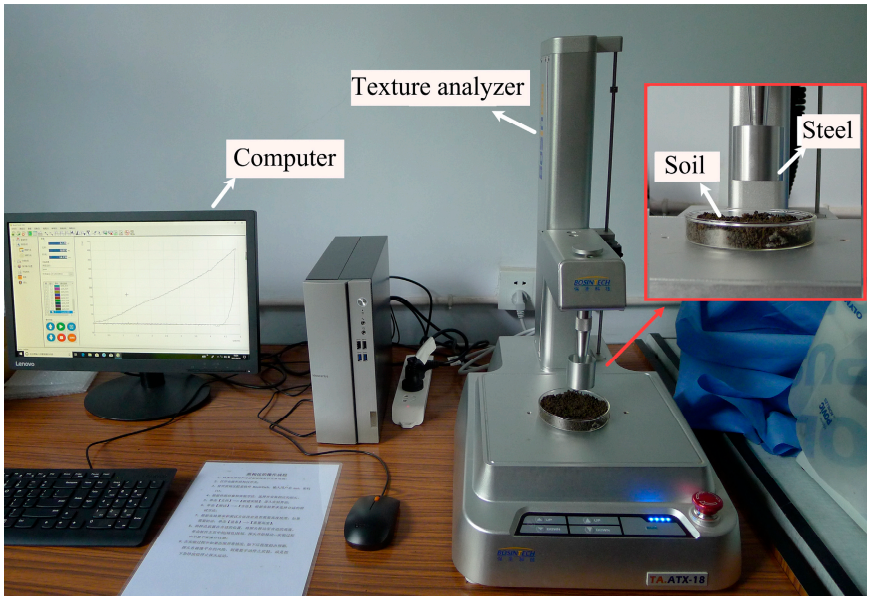

Figure 1. Analysing the adhesion of touchdown components to the soil using the TA.XTC-18 texture analyser.

2.2. Calibration of Contact Parameters Among Soil and Contact Components

In this paper, the soil with 15% water content is used as the research object, and the simulation is carried out using EDEM 2018, and the soil particle model and the parameters between the soil particles refer to the previous studies [23,24]. The parameters between the soil touching component and the soil particles are calibrated using the inclined slip test. Firstly, the Plackett–Burman test is employed to investigate the sensitivity of the contact parameters that need to be inputted manually in the EEPA model. Subsequently, the Central Composite Design test is used to calibrate and optimize these parameters.

2.2.1. Inclined Plate Slip Test of Soil Contact Parts with Soil Particles

The test set-up for the inclined slip test is presented in Figure 2. It consists of a computer, an inclined device, an inclinometer (DL1903), and a high-speed camera (Phantom v5.1). The procedure for the test was as follows: firstly, the surface angle of the inclined device is adjusted to 0 degrees, and soil particles are placed on the steel plate (boundary); then, the inclined device is rotated upwards at a certain speed until the soil particles slide down from the steel plate, and the whole process is logged with a high-speed camera; and finally, the value of the inclinometer at the moment when the soil particles slide down from the steel plate is obtained through video playback. Each set of tests is repeated three times.

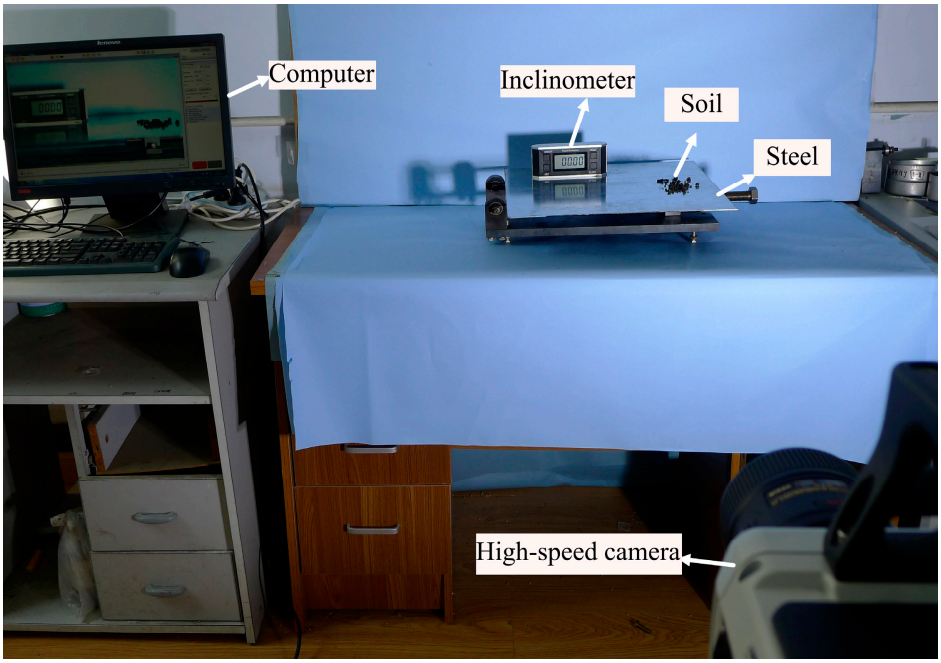

Figure 2. Sketch of the device for the inclined slip test.

2.2.2. Configuration for the Inclined Slip Tests of Contact Components with Soil Particles

In the simulation of the inclined slip test of the soil contact component with soil particles, the soil parameters are referred to as those in a previous study [24]. The procedure for the test is as follows: Firstly, soil particles are produced in the particle factory positioned above the inclined plane and remain stationary on the inclined plane, as illustrated in Figure 3. Next, the inclined plane is rotated clockwise at a speed of 8 degrees per second, and once a specific angle is attained, the soil particles move downward along the inclined plane. Finally, the inclination angle of the inclined plane is recorded when all soil particles have slid down. Each set of tests is conducted three times.

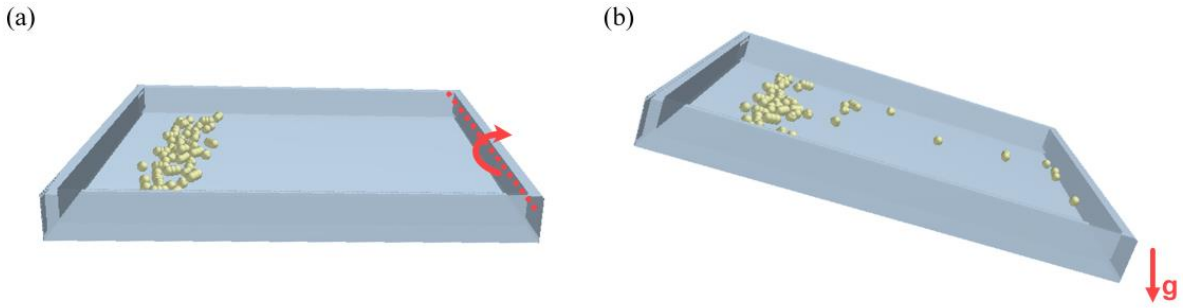

Figure 3. Simulation operation for the ramp slip test of the component with soil particles: (**a**) before rotation and (**b**) after rotation.

2.2.3. Plackett–Burman Experiment

In the Edinburgh Elasto-Plastic Adhesive (EEPA) model, the interaction parameters to be identified between the boundary and the soil particles comprise the collision recovery coefficient, coefficient of static friction, coefficient of rolling friction, surface energy, contact plasticity ratio, index of the adherence branching curves, and tangential stiffness factor, and the intervals for the seven parameters are presented in Table 1 below.

Table 1. Plackett–Burman parameter levels for slip tests between soil particles and boundaries.

Symbolic	Parameters	Low Level (−1)	High Level (+1)
X_1	Crash recovery coefficient	0.2	0.7
X_2	Coefficient of static friction	0.2	0.8
X_3	Coefficient of rolling friction	0.05	0.5
X_4	Surface energy	0.5	2
X_5	Contact plasticity ratio	0.3	0.7
X_6	Index of the adherence branching curves	1	5
X_7	Tangential stiffness factor	0.5	1
X_8–X_{11}	Virtual Parameters	—	—

2.2.4. Central Composite Design Experiment

Based on Plackett–Burman tests, sensitive parameters (static friction coefficient and surface energy) are calibrated and optimized. The upper and lower levels of static friction coefficients among the boundary and soil particles are 0.05 and 0.5, respectively, while the upper and lower levels of surface energy among the boundary and soil particles are 0.5 and 2. A coded table of factor levels for the Central Composite Design trial is shown in Table 2 below.

Table 2. Experimental design for the Central Composite Design trial.

Level	Coefficient of Static Frictions	Surface Energy, J/m^2
γ	0.4341	1.7803
1	0.5	2
0	0.28	1.25
−1	0.05	0.5
$-\gamma$	0.1159	0.7197

2.2.5. Validation of Parameter Calibration

The accuracy of the parameter calibration is verified by comparing the experimental results of the angle of repose with simulation results for soil with 15% water content. In these experiments, first, 0.4 kg of soil with a water content of 15% is placed into a galvanized rigid cylinder and the cylinder is placed on a horizontal galvanized steel plate, which is

connected to the motor using a thin wire. The motor then starts to rotate and lifts the cylinder, and the soil flows out of the cylinder and eventually piles up on the steel plate of the section, forming an angle of repose. In the simulations, the parameters obtained above are set as the parameters for EDEM simulation and the 3D model of the drum and galvanized steel sheet is built using Solid Works. The established soil particles are generated in a pellet plant at 400 g. A vertical movement is added to the drum and the particles flow out of the pile to form an angle of repose. The experimental set-up is shown in Figure 4. Lastly, the angles of repose are obtained by image fitting techniques. Three repetitions are performed for each set of trials.

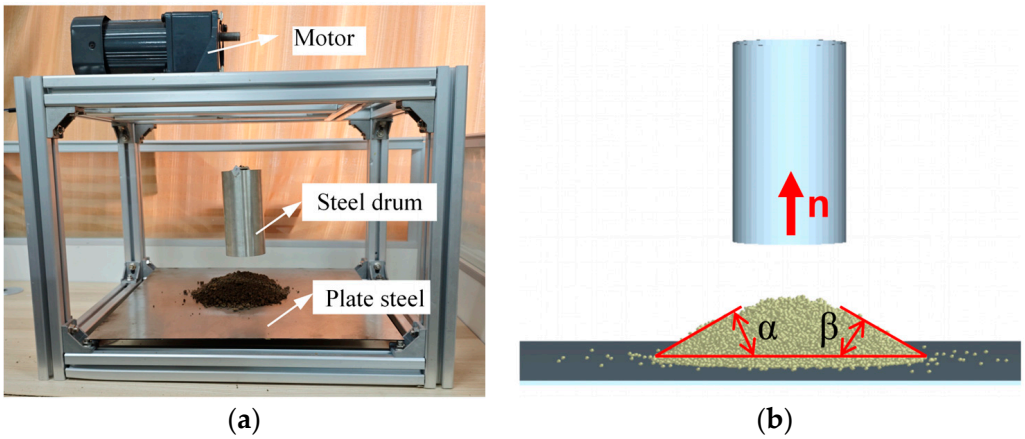

Figure 4. Measuring devices for the angle of repose: (**a**) experimental set-up and (**b**) device simulation.

2.3. Simulation of the Whole Machine of the Seeding Monomer Based on the DEM–MBD Coupling Algorithm

In the actual working process, the corn-sowing monomer moves forward in the horizontal direction under the traction of the tractor to complete the operation of ditching, seeding, covering with soil, and suppression, which involves the horizontal movement of the furrower, the levelling and rotation of the mulching disc, and the horizontal movement and rotation as well as the vertical movement of the suppressor, and the movement of the whole multi-rigid body system is complex. Therefore, it is necessary to analyse the contact process between the seeding monomer and the soil and the contact process between the seed particles and the soil using a coupled DEM–MBD algorithm. In this section, soil with a moisture content of 15 percent is used as the object of study.

2.3.1. A Multi-Body Dynamic Model of a Whole Machine Composed of the Seeding Monomer

The seeding monomer selected for this paper is a single-row corn planter with core components including a core-share furrower, a spoon-wheel seeding apparatus, a double-disc covering device, and a cylindrical suppression wheel. Among them, the core-share furrower has a front prong and a symmetrically curved surface on both sides, so that the soil rises along the curved surface, and the stubble, the top layer of dry soil pieces, moves to both sides and is overturned. It has the advantages of a simple structure, good performance when entering the soil, and a low requirement for land preparation before sowing. It is mainly used for sowing cultivated crops with wide seedling width in the ridge culture area of northeast China. For the key parameters of the core-share structure, the angle of entry of the core-share α is taken as 20 degrees; the gap angle ε is 5°; the diagonal cut angle γ is 66°; the altitude of the share H is 140 mm; and the size of width B depends on the seedling width of the seedling sowing, which is taken as 120 mm, as shown in Figure 5.

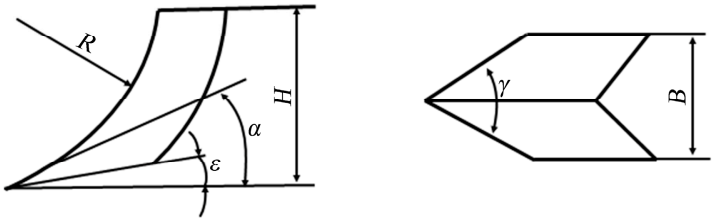

Figure 5. Core-share structure.

The spoon-wheel seeding apparatus consists of a planter plate, seed guide wheel, separator, seed-metering wheel, and seed planter cover as shown in Figure 6.

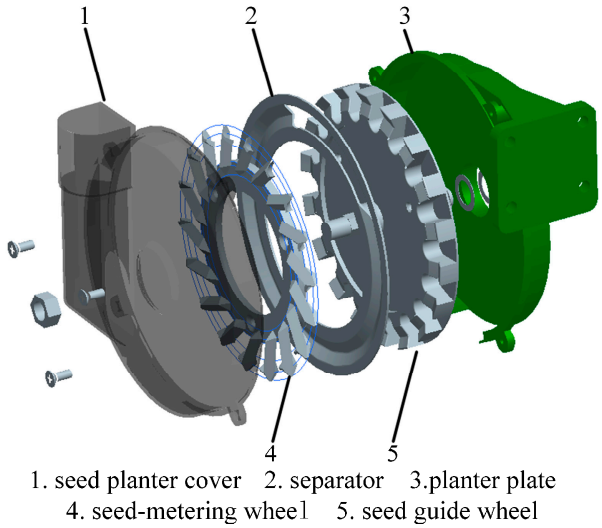

Figure 6. Spoon-wheel seeding apparatus.

The covering device is a double sealer, mostly used in conjunction with a core-share furrower, which has the advantages of large mulching volume, strict covering, and low operating resistance. The covering device has a diameter of 300 mm and a 40° angle of opening. In addition, the cylindrical roller has a diameter of 260 mm.

The 3D model of the whole machine composed of the seeding monomer established by ProE is shown in Figure 7. The seeding unit interacts with the soil and undergoes levelling under the traction of the tractor; the front beam is connected to the traction frame by an articulated connection and pre-tensioned by springs, and the furrower is fixed under the front beam; the seeding apparatus is fixedly connected to the front beam, and the seeding apparatus is connected to the seeding plate shaft by an articulated connection; the rear beam is fixedly connected to the front beam, the linking bar of the covering device is pivotally connected to the front beam and preloaded with the rear beam using a spring, and the covering device is pivotally connected to the covering device linking bar bracket; and the connecting rod of the packer wheel is pivotally connected to the rear beam and pre-tensioned by a spring, and the packer wheel is pivotally connected to the packer wheel connecting rod. Therefore, there are 7 articulated connections and 4 fixed connections in the seeding monomer. The model of the seeding monomer is stored in the STP format and introduced into RecurDyn to establish the constraint model of the seeding monomer, as shown in Figure 8.

A substantial portion of the entire seeding unit is steel, so in RecurDyn, set the properties of each part to 'Steel', and set the connection types between the rigid bodies involved in the machine, see Table 3.

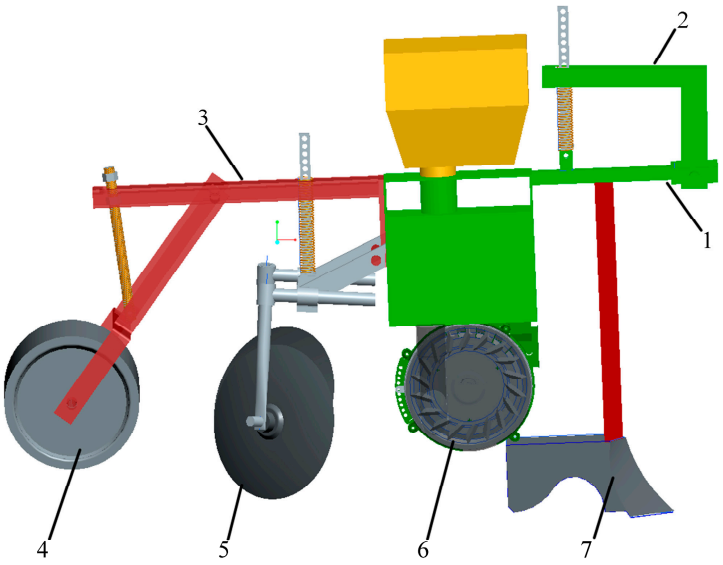

1. front beam 2. traction frame 3. rear beam 4. packer wheel 5. covering device 6. seeding apparatus 7. furrower

Figure 7. Three-dimensional model of the seeding monomer.

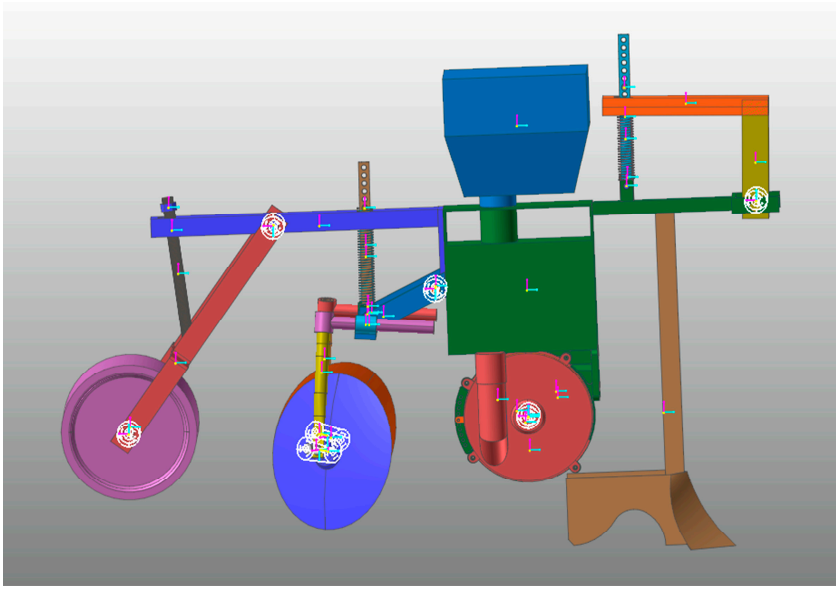

Figure 8. Analytical model for the seeding monomer in RecurDyn.

Table 3. Constraint types among rigid bodies in the seeding monomer.

Constraint Sequence Number	Targets of Constraint	Types of Constraint
1	Hanger and front beam	Revolve pair
2	Furrower–ground	Revolve pair
3	Seed-metering wheel–seed-metering shafts	Revolve pair
4	Covering device linkage bar—front beam	Revolve pair
5	Covering discs—covering connections	Revolve pair
6	Packer wheel connecting rod—rear beam	Revolve pair
7	Packer wheel connecting rod—covering device	Revolve pair

After setting the constraint method, the parts of the whole machine without constraints and fixed connections are combined. In the case of DEM–MBD coupling, the files are in the form of a wall to achieve data transfer, so it is necessary to output each part of the whole machine as a wall file in RecurDyn software (V9R4), and the parts cannot be duplicated among each other.

To apply drive to the seeding monomer, this paper compares and analyses the simulation results with the experimental results of Xu [25], and sets the drive mode as speed drive, with a total of three groups of different speeds in the simulation; the speeds are 0.75 m/s, 1.11 m/s, and 1.47 m/s, and the direction is the +X direction.

2.3.2. EDEM Simulation Set-Up and Coupling Calculation

The soil slot is generated in EDEM and the dimensions of the soil slot are determined to be 4.82 m × 0.42 m × 0.82 m based on the spacing of the maize sowing plants (a plant spacing of about 24 cm) and the overall dimensions of the seeding monomer. The parameters between the soil and maize seed are selected based on previous studies [23,24].

The block factory in EDEM software (2018) is used to generate the soil slot for simulation, as shown in Figure 9.

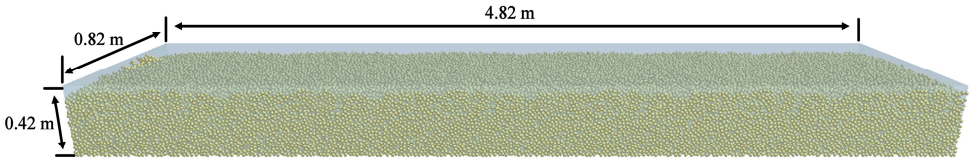

Figure 9. Soil slots generated in EDEM software.

A coupled simulation using EDEM and RecurDyn is used to analyse the process of ditching seeding and covering with soil and suppression. After completing the above basic settings, enter the coupling calculation mode, open the coupling service in EDEM by clicking Coupling Server, set the simulation time step of RecurDyn and EDEM to 3×10^{-4} and 9×10^{-6}, respectively, and select 5 s for the simulation time to start the coupling calculation. Screenshots of the simulation interfaces of the two software at different simulation moments after entering the coupling are shown in Figures 10–12.

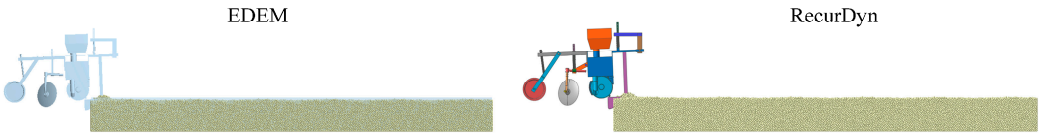

Figure 10. Simulation interface of the two software when the simulation time is 0.15 s.

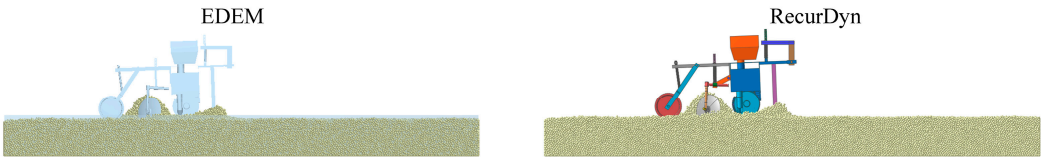

Figure 11. Simulation interface of the two software when the simulation time is 1.5 s.

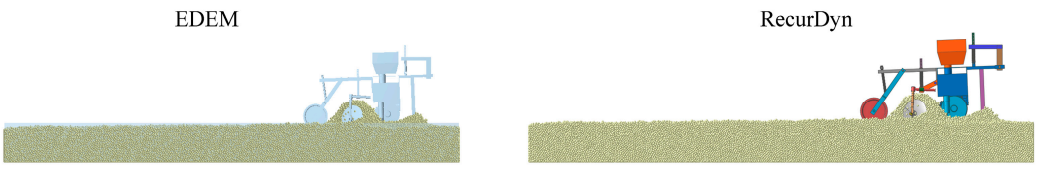

Figure 12. Simulation interface of the two software when the simulation time is 3 s.

2.3.3. Simulation Examination of the Ditching Procedure of the Seeding Unit

The seeding monomer moves forward in the horizontal direction under the action of the speed drive with the speed magnitude taking the values of 0.75 m/s, 1.11 m/s, and 1.47 m/s, respectively. In this section, the influence of the seeding monomer on the ditching of the furrower at different advancing speeds is studied.

2.3.4. Simulation Examination of the Covering with Soil Procedure of the Seeding Unit

In this section, the effect of the covering with soil process on seed position at different forward speeds is investigated. The positional changes of seeds before and after covering with soil with different shapes of seed particles at different forward speeds of the seeding monomer (longitudinal, transverse, and sowing depth directions) were studied. The findings are subsequently contrasted with Xu's [25] experimental results during the soil-covering process.

The technique for determining the alteration in the seed's position before and after being covered with soil (longitudinal, transverse, and sowing depth direction) is as follows: firstly, after the seed falls into the seed furrow and stabilizes in the EDEM software, the Geometry bin is established according to the position of the selected seed, and this simulation time t_1 is recorded, see Figure 13; then, when the covering device of the seeding monomer buries the seed into the soil, the simulation time t_2 is recorded at this time; and finally, the position of the seed in the period t_1~ t_2 is exported, to calculate the location variation of the seed in the longitudinal, transverse, and sowing depth directions before and after covering with soil.

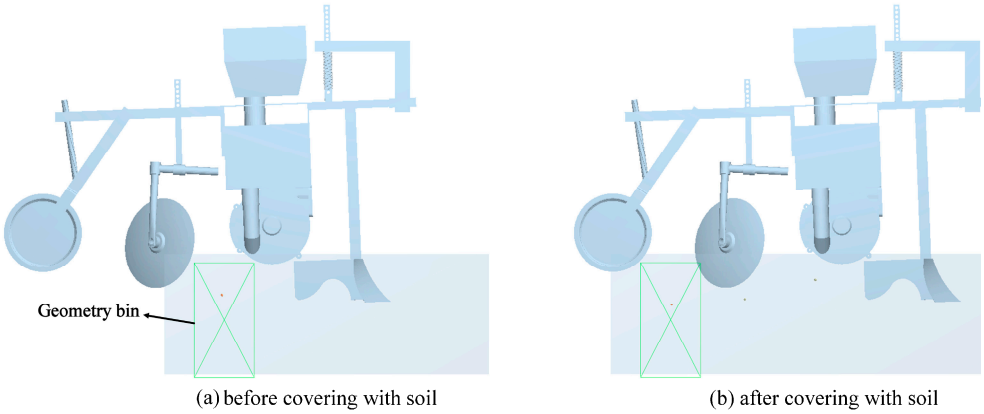

Figure 13. Calculation of the variation in the location of the seed in the longitudinal, transverse, and sowing depth directions before and after covering with soil.

2.3.5. Simulation Study of the Suppression Procedure of the Seeding Unit

In this section, the relationship between the process of suppression and seed displacement at different forward speeds is investigated. The changes in the position of seeds before and after suppression with different shapes of seed particles at various forward speeds of the seeding unit are analysed by simulation. Then, the results are compared with the experimental results of Xu [25] in the suppression process.

The method of obtaining the position change of seeds before and after suppression (longitudinal, transverse, and sowing depth direction) is as follows: firstly, in EDEM software, after the seeds are buried in the soil by the covering device, the Geometry bin is established according to the position of the selected seeds, and the simulation time t_3 of this simulation is recorded, see Figure 14; then, after the press roller of the seeding monomer is rolled over the top of the seeds, the simulation time at this time t_4 is recorded; and finally, the position of the seed in the longitudinal, transverse, and sowing depth directions in the period t_3~t_4 is exported through EDEM software, to calculate the position

changes of the seed in the longitudinal, transverse, and sowing depth directions before and after suppression.

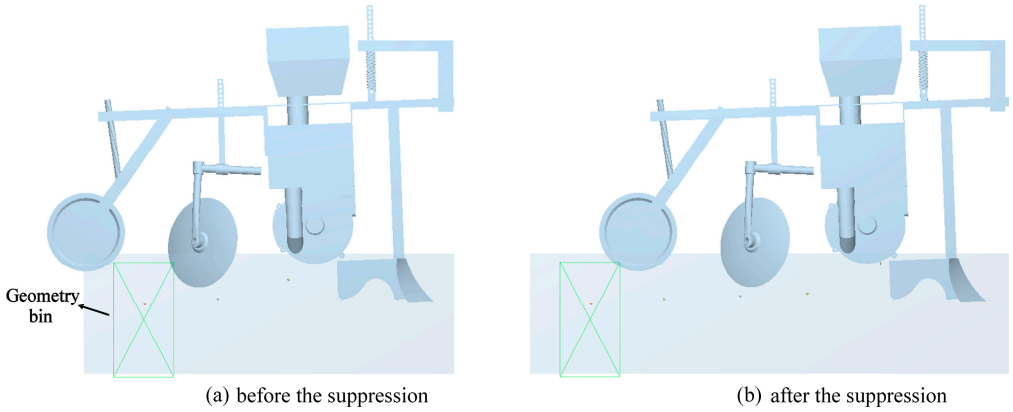

Figure 14. Calculation of change in seed position in longitudinal, transverse, and sowing depth directions before and after suppression.

2.3.6. Sowing Uniformity

In this section, the effect of seeding uniformity at different forward speeds of the seeding monomer is analysed by simulation. Figures 15–17 show the distribution of maize seeds at the three operating speeds. The mean and the standard deviation of the longitudinal grain spacing are calculated by counting the longitudinal positions between the particles of the seeds after covering with soil and suppression. The uniformity of seeding is expressed by the ratio of the mean and standard deviation of the longitudinal grain spacing.

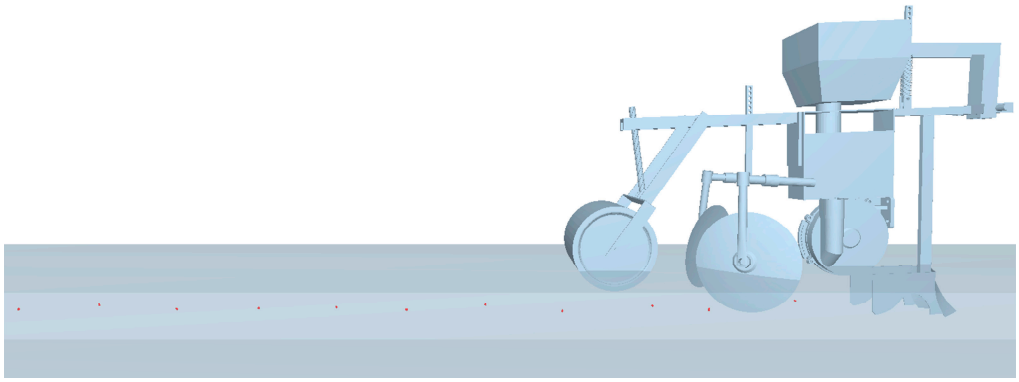

Figure 15. Distribution of maize seeds at a seeding monomer forward speed of 0.75 m/s.

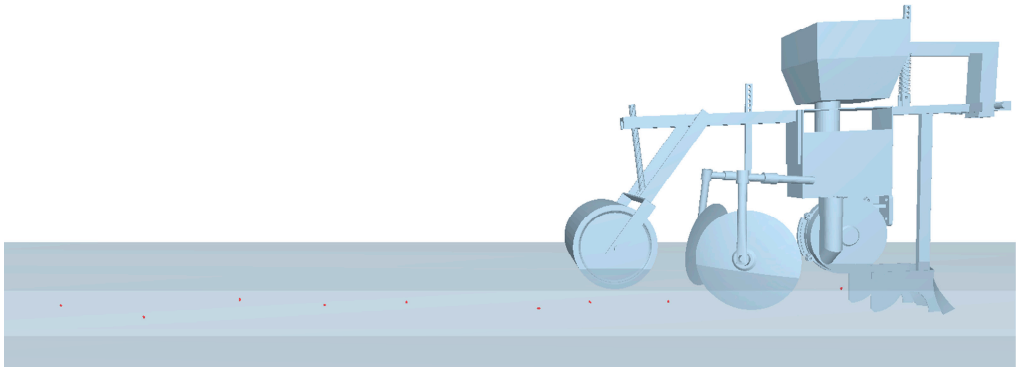

Figure 16. Changes in seed position at a seeding unit forward speed of 1.11 m/s.

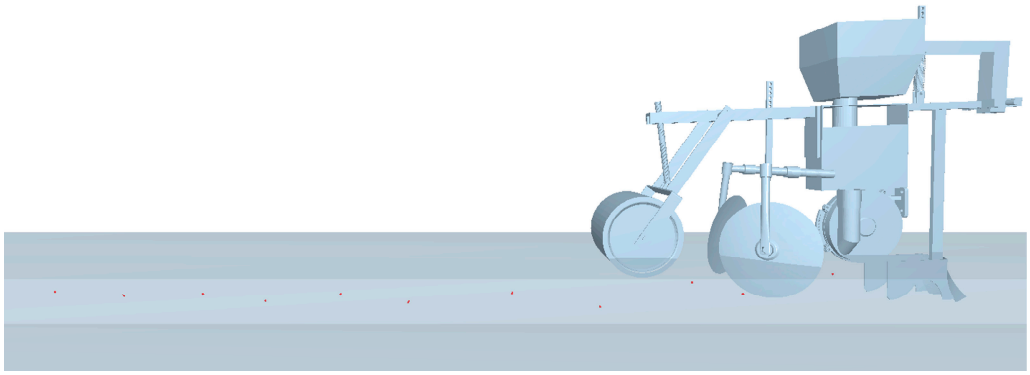

Figure 17. Distribution of maize seeds at a seeding unit forward speed of 1.47 m/s.

3. Results and Discussion

3.1. Results of the Selection of a Contact Model Between Soil and Soil Contact Components

The curves illustrating the relationship between force and displacement for three different levels of soil moisture in normal contact with the boundary are depicted in Figure 18. Here, "gf" is used as the unit of force, representing the force of gravity on an object with a mass of 1 g. It is important to note that the horizontal axis of the graph denotes the variation in probe displacement, whereas the vertical axis signifies the magnitude of the contact force between the probe and the soil. Additionally, the maximum negative force on the graph represents the peak adhesion of the soil to the probe.

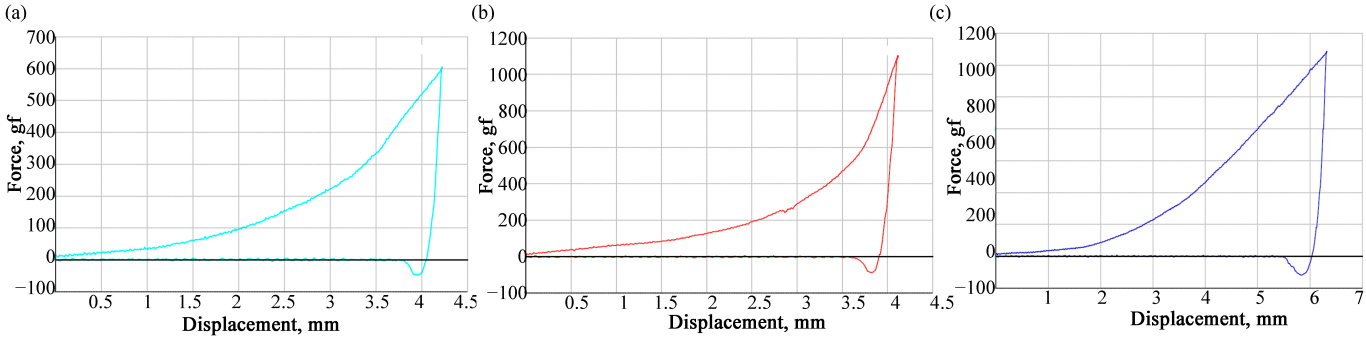

Figure 18. Variation curves of normal contact force versus displacement between soil and component at different water contents: (**a**) 15%, (**b**) 20%, and (**c**) 25%.

The test statistics are counted to obtain the maximum adhesion force, and based on the contact area, the magnitude of the pressure for the adhesion effect is calculated. It can be concluded that when the soil water content is 15%, the peak adhesion is 0.644 N, and the calculated magnitude of pressure is 911.691 pa; when the soil contains 20% moisture, the greatest level of soil sticking to the boundary is measured at 0.664 N, and the calculated magnitude of pressure is 940.217 pa; and when the soil contains 25%, the peak adhesion is 1.326 N and the calculated magnitude of the pressure is 1877.160 pa. Therefore, for the contact between the boundary and the soil, the presence of adhesion forces needs to be considered, which can have a significant effect on the boundary–soil interaction process. Furthermore, while it is possible to substitute the shear adhesion force by enhancing the coefficients of static and rolling friction, the normal adhesion force cannot be offset using this method.

To summarise, the EEPA model has been chosen for the boundary–soil contact model in this paper.

3.2. Calibration Results of Contact Parameters Among Soil and Contact Components

3.2.1. Plackett–Burman Experimental Program and Analysis of Results

The design scheme of the Plackett–Burman test and the results of the test are shown in Table 4 below.

Table 4. Results of Plackett–Burman test for slip test between soil particles and boundary.

Test Sequences	X_1	X_2	X_3	X_4	X_5	X_6	X_7	X_8	X_9	X_{10}	X_{11}	Angles, Deg
1	1	1	−1	1	1	1	−1	−1	−1	1	−1	74.40
2	−1	1	1	−1	1	1	1	−1	−1	−1	1	59.36
3	1	−1	1	1	−1	1	1	1	−1	−1	−1	16.48
4	−1	1	−1	1	1	−1	1	1	1	−1	−1	60.24
5	−1	−1	1	−1	1	1	−1	1	1	1	−1	18.00
6	−1	−1	−1	1	−1	1	1	−1	1	1	1	25.84
7	1	−1	−1	−1	1	−1	1	1	−1	1	1	15.76
8	1	1	−1	−1	−1	1	−1	1	1	−1	1	42.08
9	1	1	1	−1	−1	−1	1	−1	1	1	−1	44.08
10	−1	1	1	1	−1	−1	−1	1	−1	1	1	62.00
11	1	−1	1	1	1	−1	−1	−1	1	−1	1	23.36
12	−1	−1	−1	−1	−1	−1	−1	−1	−1	−1	−1	5.60
13	0	0	0	0	0	0	0	0	0	0	0	38.24

The test results are then analysed by variance to derive the degree of influence of each test parameter on the slip angle, as shown in Table 5 below.

Table 5. Analysis of variance for the Plackett–Burman test.

Origins	Square Sum	Freedom	Mean Square	F-Values	*p*-Values	
Modelling	4942.35	7	706.05	19.12	0.0025	significant
X_1	51.58	1	51.58	1.4	0.2904	
X_2	4298.62	1	4298.62	116.39	0.0001 **	
X_3	9.43	1	9.43	0.26	0.6348	
X_4	379.01	1	379.01	10.26	0.0239 *	
X_5	169.05	1	169.05	4.58	0.0854	
X_6	19.05	1	19.05	0.52	0.5048	
X_7	15.6	1	15.6	0.42	0.5445	
Residual	184.67	5	36.93			
Total deviation	5127.02	12				

Note: ** indicates that the item is highly significant ($p < 0.01$), and * indicates that the item is significant ($p < 0.05$).

From the experimental results of the Plackett–Burman test, it can be seen that the coefficient of static friction between the soil and the boundary ($p < 0.01$) has an extremely significant influence on the slip test, and the surface energy has a noteworthy influence on the slip test ($p < 0.05$). For the other parameters, a collision recovery coefficient of 0.5, a rolling friction coefficient of 0.05, a contact plasticity ratio of 0.6, an index of the adherence branching curve of 3, and a tangential stiffness factor of 0.67 are taken from Refs. [26–28].

3.2.2. Analysis of Central Composite Design Test Results

The Central Composite Design experimental design and results are shown in Table 6 below.

Table 6. Central Composite Design experimental design and results.

Test Sequences	Coefficient of Static Friction (X_2)	Surface Energy, J/m^2 (X_4)	Angles, Deg
1	−1	−1	11.28
2	1	−1	31.60
3	−1	1	17.12

Table 6. *Cont.*

Test Sequences	Coefficient of Static Friction (X_2)	Surface Energy, J/m^2 (X_4)	Angles, Deg
4	1	1	41.92
5	−1.41	0	6.56
7	0	−1.41	20.56
8	0	1.41	37.04
9	0	0	28.88
10	0	0	28.72
11	0	0	23.60
12	0	0	30.56
13	0	0	31.44

From the test results shown in the table, the regression equations are obtained as follows, with the static friction coefficient (X_2) and surface energy (X_4) as independent variables and the slip angle (Y) as the response value:

$$Y = 28.64 + 10.26X_2 + 4.93X_4 + 1.12X_2X_4 - 4.19{X_2}^2 + 0.4{X_4}^2 \quad (2)$$

where the slip angle is represented by Y; the static friction coefficient and surface energy are represented by X_2 and X_4, respectively.

The consequences of the tests are analysed using an ANOVA, and the findings are presented in Table 7 below.

Table 7. Variance consequences for the Central Composite Design trial.

Origins	Squares	Freedom	Mean Square	F-Values	*p*-Values	
Modelling	1170.69	5	234.14	29.91	0.0001	significant
X_2	842.88	1	842.88	107.66	<0.0001 **	
X_4	194.70	1	194.70	24.87	0.0016 **	
X_2X_4	5.02	1	5.02	0.64	0.4497	
${X_2}^2$	121.84	1	121.84	15.56	0.0056	
${X_4}^2$	1.09	1	1.09	0.14	0.7207	
Parameters	54.80	7	7.83			
Lack of fit items	17.81	3	5.94	0.64	0.6272	insignificant
Error terms	36.99	4	9.25			
Total deviation	1225.50	12				

Note: ** indicates that the item is highly significant ($p < 0.01$).

As can be seen from the data in the table, in the regression model with $p < 0.0001$, the difference reached a highly significant level, and the level of the lack of fit items is not significant ($p > 0.05$), which indicates that the equation is well fitted. The above findings indicate the feasibility of applying a modified mathematical model to characterize the degree of influence of the factors on the response values.

In addition, as can be seen from the table, X_2 (static friction coefficient) and X_4 (surface energy) have extremely significant effects on the angle of repose ($p < 0.01$), and among the secondary terms, ${X_2}^2$ has a highly significant effect on the angle of repose ($p < 0.01$); among the interaction terms, none of them has a significant interaction ($p > 0.05$).

The response surface plots between the factors are obtained based on the quadratic regression equation, which leads to the interaction between the factors and the optimal parameter combinations. From Figure 19, it can be seen that the optimal parameters exist within the designed range of factor levels.

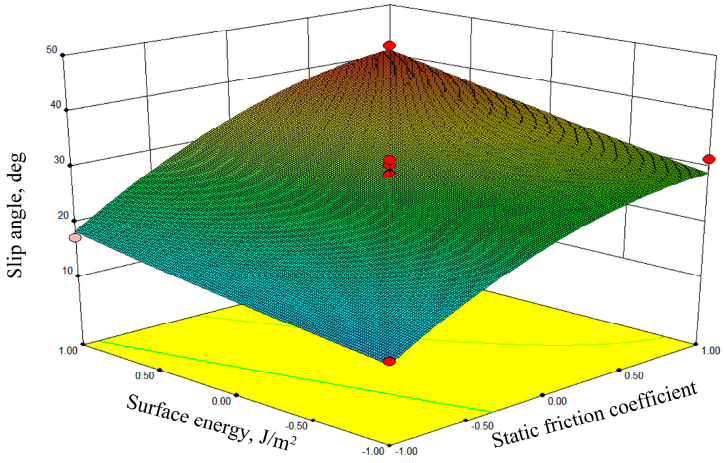

Figure 19. Response surface plots of the interaction of the factors on the effect of slip angle.

The use of statistical analysis software to optimize the developed mathematical model yielded an ideal set of parameters for soil with a moisture content of 15%. Specifically, this includes a static friction coefficient of 0.48 between the soil and its boundary, along with a surface energy measure of 1.82.

3.2.3. Analysis of the Results of Parameter Calibration

The results from both the test and simulation are illustrated in Figure 20. The value of the angle of repose is obtained by image fitting. The proportional error among the simulation results of the angle of repose and the experimental results is 4.37%, which verifies the accuracy of the parameter calibration. Based on the data presented in the table, it is evident that the magnitude of the angle of repose is similar between the experimental and simulation results. This similarity demonstrates the accuracy of the parameter calibration described above.

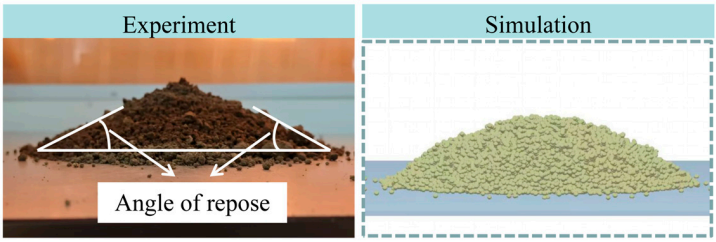

Figure 20. Illustration of the angle of repose.

3.3. Analysis of Simulation Results of the Whole Seeding Monomer Machine Based on DEM and MBD Coupling Algorithm

3.3.1. Analysis of Simulation Results of the Furrowing Process of the Seeding Monomer

Figure 21 shows the furrow shape at various forward speeds of the seeding monomer; the shape of the seed channel is binarized, and the coordinates of the points are obtained to obtain the contour of the seed channel (Figure 22).

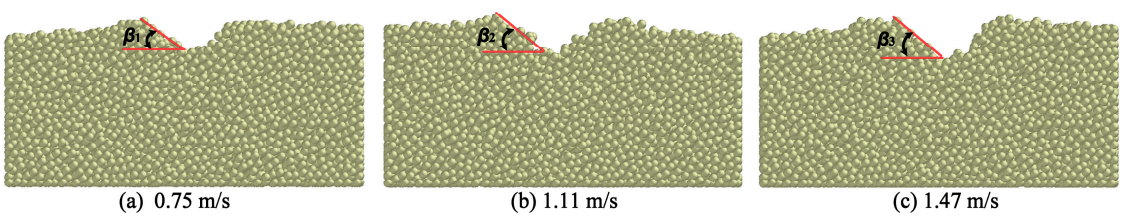

Figure 21. Shape of seed furrows formed by seeding unit at three speeds.

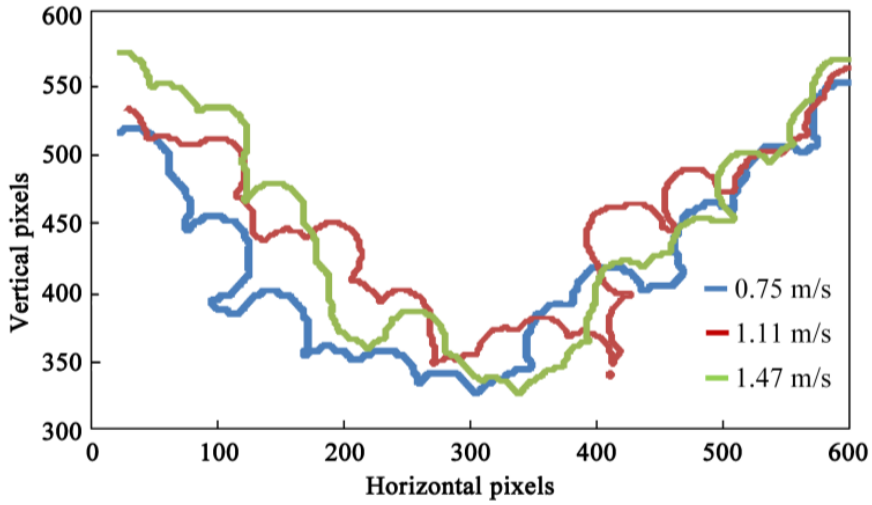

Figure 22. Contours of the shape of the seed channel at three speeds of the seeding monomer.

As can be seen in Figure 22, there is a significant difference in the contours of the seed channel at different speeds. Further, the slopes of the seed channel at different forward speeds are measured using an image recognition method, and the consequences are presented in Figure 23. From the figure, it can be seen that the slope of the seed channel increases as the forward speed increases.

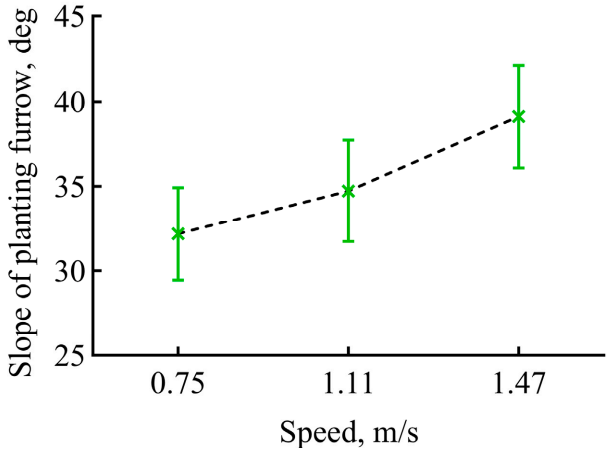

Figure 23. Results of the slopes of the seed channel at different forward speeds.

3.3.2. Analysis of the Simulation Results for the Covering with Soil Process of the Seeding Monomer

The variations in the location of the seeds of different shapes before and after the covering with soil at various forward speeds of the seeding unit are shown in Figure 24, from which it can be seen that the displacement of the seed particles of various shapes in the longitudinal direction increased significantly with the rise in the forward speed of the seeding unit, whereas the displacements of the seeds in the transversal direction and the direction of the sowing depth decreased with the increase in the forward speed of the monomer. Moreover, since the trends of seed particles of all shapes in the transverse and longitudinal directions as well as in the direction of sowing depth are the same, it can be concluded that the perturbation of seed displacement by the process of covering with soil is independent of seed shape.

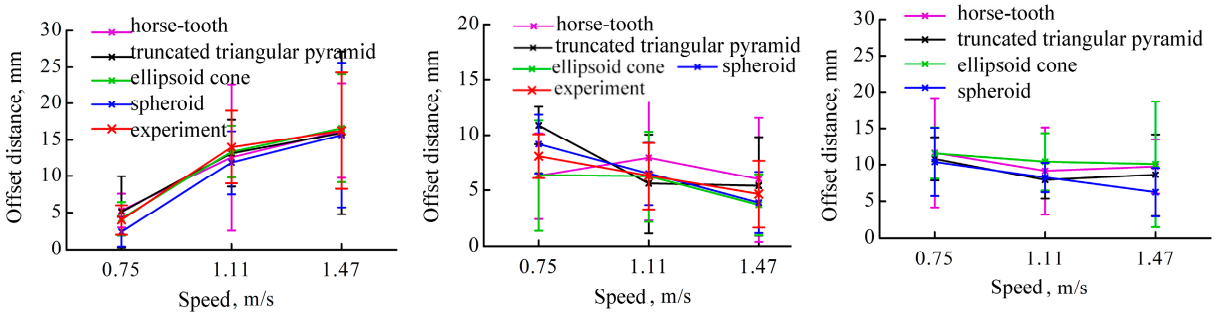

Figure 24. Seed position offset for each shape before and after coverage at different forward speeds.

In addition, the simulation results of each shape of seed particles are compared with the experimental results of Xu's [25] process of covering with soil. It can be seen from Figure 24 that the simulation results exhibit the same trend of change as the experimental results and the relative error between the simulation and experimental results is within 23.5%.

3.3.3. Analysis of the Simulation Results for the Suppression Process of the Seeding Monomer

Figure 25 shows the change in seed position before and after the suppression of differently shaped seed particles at different forward speeds of the seeding monomer. From the graph, it can be obtained that the dislocation of the seed particles of each shape in the longitudinal and transverse directions gradually increases as the forward speed of the seeding unit rises, and the displacement of the seed particles of each shape in the direction of the sowing depth decreases. Moreover, because the variation trend of seed particles of different shapes is the same in the direction of horizontal, vertical, and sowing depth, it can be concluded that the disturbance of seed displacement during the process of suppression is independent of seed shape. In addition, the simulation results of each shape of seed particles are compared with the experimental results of Xu's [25] process of suppression. It can be seen from Figure 25 that the changing trend of the simulation results and the experimental results are consistent, and the relative error between the simulation and experimental results is within the standard deviation of the experimental results.

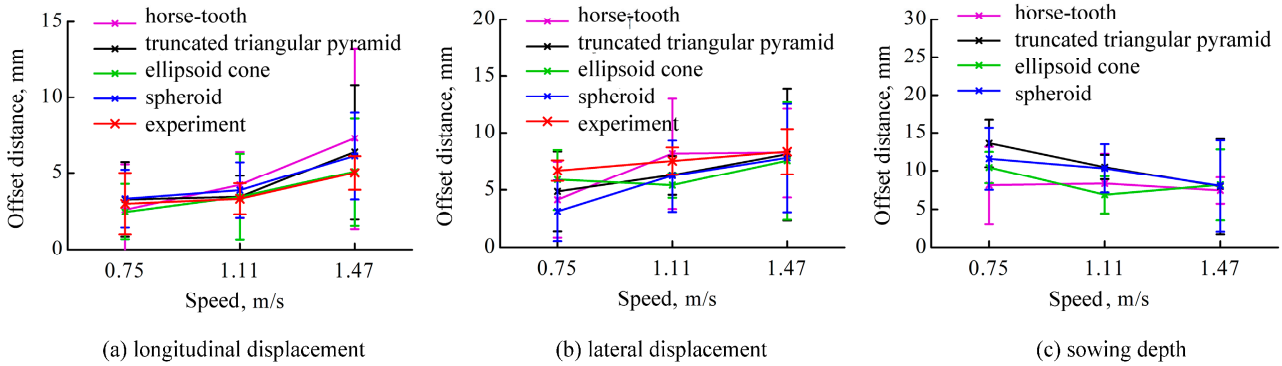

Figure 25. Seed position offset for each shape before and after compaction at different forward speeds.

3.3.4. Sowing Uniformity Analysis

Figure 26 shows the uniformity of the longitudinal grain spacing of maize seeds at three operating speeds of the seeding monomer. As can be seen from the figure, the sowing uniformity decreases as the operating speed increases.

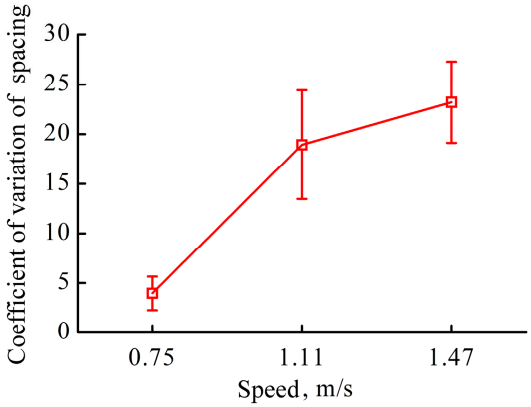

Figure 26. Uniformity of sowing at different forward speeds of the seeding monomer.

4. Conclusions

In this article, the interaction process among soil and contact components is investigated, the contact model among soil and components is determined, and the contact parameters among soil and components therein are calibrated. The coupled computational method of DEM–MBD is employed to analyse the covering with soil and the suppression process of the seeding monomer. The relevant conclusions are as follows.

(1) By studying the vertical contact between the boundary (galvanized steel) and the soil, the effect of the adhesion of the soil to the boundary on the contact process is obtained. The results showed that for the contact between the boundary and the soil, the presence of adhesion forces needs to be considered, which can have a significant effect on the boundary–soil contact process. In addition, the presence of shear adhesion force can be substituted by growing the coefficient of static friction and the coefficient of rolling friction, but the normal adhesion force cannot be compensated in this way.

(2) The positional alterations of seed particles possessing various shapes—along their length, width, and depth—are examined both prior to and following their covering with soil. This examination occurs at differing forward velocities of the seeding apparatus and is conducted via simulation. The results show that the displacement of seed particles of different shapes in the longitudinal direction increased significantly with the increase in the forward speed of the seeding monomer, while the displacement of seed particles in the transverse direction and the sowing depth direction decreased with the increase in the forward speed of the monomer. Moreover, the disturbance of seed displacement by the covering with soil process is independent of seed shape.

(3) The positional changes of seeds of different shapes before and after suppression under different forward speeds of the seeding monomer are analysed by simulation, and the results show that with the increase in the forward speed of the seeding monomer, the displacements of seed particles of various shapes in the longitudinal and transverse directions gradually increase, and the displacements of seed particles of various shapes in the direction of the sowing depth decrease. Moreover, the perturbation of seed displacement by the suppression process is independent of seed shape.

(4) The effect of sowing uniformity under different forward speeds of the seeding monomer is analysed by simulation, and the results show that the sowing uniformity of maize seeds decreases with the increase in operating speed.

Author Contributions: Conceptualization, L.Z. and K.S.; methodology, L.Z.; software, C.H.; validation, Q.Z., X.Y., Q.D. and W.W.; formal analysis, Y.C.; investigation, M.L. and X.X.; resources, L.Z.; data curation, Y.W.; writing—original draft preparation, K.S.; writing—review and editing, L.Z.; visualization, K.S.; supervision, Q.D.; project administration, L.Z.; funding acquisition, L.Z. All authors have read and agreed to the published version of the manuscript.

Funding: The authors are grateful to the Natural Science Foundation of Shandong Province (grant number ZR2023QE198, ZR2023QF143), the National Natural Science Foundation of China (grant number 52405280, 52130001), the Shandong Province Agricultural Machinery R&D, Manufacturing and Promotion Application Integration Pilot Project (Grant No. NJYTHSD-202315), and the Science and Technology Support Plan for Youth Innovation of Colleges and Universities of Shandong Province of China (grant number 2022KJ225) for the financial support of this work.

Data Availability Statement: The original contributions presented in the study are included in the article, further inquiries can be directed to the corresponding author(s).

Conflicts of Interest: The authors declare no conflicts of interest.

References

1. Zhang, S.; Hao, X.; Wang, Z.; Cui, A.; Chen, S. Interactive Effects of Different Combination of Row Spacing and Plant Distance on the Yield and Yield Components of Summer Maize. *Chin. Agric. Sci. Bull.* **2013**, *29*, 51–56.
2. Wang, W.; Ma, X.; Yuan, R.; Yuan, Y.; Wang, J. Experimental Study on Displacement of Seed Bounce and Rolling Based on Uniform Design. *J. Jilin Agric. Univ.* **2006**, *28*, 694–696.
3. Wang, J. The Research of Position Control after Seed Contacting Soil in the Process of Soil Covering and Rolling with Precision Seeder. Ph.D. Thesis, Jilin University, Changchun, China, 2012.
4. Cundall, P.A.; Strack, O.D.L. A discrete numerical model for granular assemblies. *Geotechnique* **1979**, *29*, 47–65. [CrossRef]
5. Yuan, F.; Yu, H.; Wang, L.; Shi, Y.; Wang, X.; Liu, H. Parameter Calibration and Systematic Test of a Discrete Element Model (DEM) for Compound Fertilizer Particles in a Mechanized Variable-Rate Application. *Agronomy* **2023**, *13*, 706. [CrossRef]
6. Wang, F.; Dai, F.; Zhang, F.; Song, X.; Shi, R.; Zhao, W.; Ma, H. Simulation Analysis and Test on the Effect of Picking Up the Residual Film of Typical Film Lifting Parts. *Agronomy* **2023**, *13*, 488. [CrossRef]
7. Walunj Avdhoot Chen, Y.; Tian, Y.; Zeng, Z. Modeling Soil–Plant–Machine Dynamics Using Discrete Element Method: A Review. *Agronomy* **2023**, *13*, 1260. [CrossRef]
8. Zhao, H.; Huang, Y.; Liu, Z.; Liu, W.; Zheng, Z. Applications of Discrete Element Method in the Research of Agricultural Machinery: A Review. *Agriculture* **2021**, *11*, 425. [CrossRef]
9. Yan, D.; Yu Jn Wang, Y.; Zhou, L.; Tian, Y.; Zhang, N. Soil Particle Modeling and Parameter Calibration Based on Discrete Element Method. *Agriculture* **2022**, *12*, 1421. [CrossRef]
10. Chen, Y.; Munkholm Lars, J.; Nyord, T. A discrete element model for soil–sweep interaction in three different soils. *Soil Tillage Res.* **2013**, *126*, 34–41. [CrossRef]
11. Hang, C.; Huang, Y.; Zhu, R. Analysis of the movement behavior of soil between subsoilers based on the discrete element method. *J. Terramech.* **2017**, *74*, 35–43. [CrossRef]
12. Wang, Y.; Zhang, D.; Yang, L.; Cui, T.; Jing, H.; Zhong, X. Modeling the interaction of soil and a vibrating subsoiler using the discrete element method. *Comput. Electron. Agric.* **2020**, *174*, 105518. [CrossRef]
13. Sun, J.; Chen, H.; Wang, Z.; Ou, Z.; Yang, Z.; Liu, Z.; Duan, J. Study on plowing performance of EDEM low-resistance animal bionic device based on red soil. *Soil Tillage Res.* **2020**, *196*, 104336. [CrossRef]
14. Ahmad, F.; Qiu, B.; Ding, Q.; Ding, W.; Mahmood, K.; Shoaib, M. Ali Chandio Farman, Rehim Abdur, Khaliq Abdul. Discrete element method simulation of disc type furrowers in paddy soil. *Int. J. Agric. Biol. Eng.* **2020**, *13*, 103–110.
15. Wang, X.; Zhang, S.; Pan, H.; Zheng, Z.; Huang, Y.; Zhu, R. Effect of soil particle size on soil-subsoiler interactions using the discrete element method simulations. *Biosyst. Eng.* **2019**, *182*, 138–150. [CrossRef]
16. Ucgul, M.; Fielke, J.M.; Saunders, C. Three-dimensional discrete element modeling (DEM) of tillage: Accounting for soil cohesion and adhesion. *Biosyst. Eng.* **2015**, *129*, 298–306. [CrossRef]
17. Barr, J.B.; Ucgul, M.; Desbiolles Jack, M.A.; Fielke John, M. Simulating the effect of rake angle on narrow opener performance with the discrete element method. *Biosyst. Eng.* **2018**, *171*, 1–15. [CrossRef]
18. Barr, J.; Desbiolles, J.; Ucgul, M.; Fielke John, M. Bentleg furrower performance analysis using the discrete element method. *Biosyst. Eng.* **2020**, *189*, 99–115. [CrossRef]
19. Mak, J.; Chen, Y.; Sadek, M.A. Determining parameters of a discrete element model for soil–tool interaction. *Soil Tillage Res.* **2012**, *118*, 117–122. [CrossRef]
20. Xing, W.; Zhang, H.; Sun, W.; Li, H.; Liu, X.; Li, H.; Chen, Y.; Lu, Y. Performance Study of a Chain–Spoon Seed Potato Discharger Based on DEM-MBD Coupling. *Agriculture* **2024**, *14*, 1520. [CrossRef]
21. Fang, W.; Wang, X.; Han, D.; Zang, N.; Chen, X.; Ohiemi, I.E. Parameter optimization and disturbance analysis of the film picking device of the chain-type plough layer residual film recovery machine based on DEM-MBD coupling. *Comput. Electron. Agric.* **2024**, *222*, 109041. [CrossRef]
22. Xie, D.; He, J.; Liu, T.; Liu, C.; Zhao, G.; Chen, L. Establishment and validation the DEM-MBD coupling model of flexible straw-Shajiang black soil-walking mechanism interactions. *Comput. Electron. Agric.* **2024**, *224*, 109203. [CrossRef]
23. Zhou, L.; Dong, Q.; Yu, J.; Wang, Y.; Chen, Y.; Li, M.; Wang, W.; Yu, Y.; Yuan, J. Validation and Calibration of Maize Seed–Soil Inter-Parameters Based on the Discrete Element Method. *Agronomy* **2023**, *13*, 2115. [CrossRef]

24. Zhou, L.; Lan, Y.; Yu, J.; Wang, Y.; Yan, D.; Sun, K.; Wang, W.; Chen, Y. Validation and calibration of soil parameters based on EEPA contact model. *Comput. Part. Mech.* **2023**, *10*, 1295–1307. [CrossRef]
25. Xu, T. Experimental Study and Simulation Analysis of the Working Process of the Precision Seeding Unit and Its Key Parts. Ph.D. Thesis, Jilin University, Changchun, China, 2019.
26. Sun, W.; Sun, Y.; Wang, Y.; He, H. Calibration and experimental verification of discrete element parameters for modelling feed pelleting. *Biosyst. Eng.* **2024**, *237*, 182–195. [CrossRef]
27. Wu, Z.; Wang, X.; Liu, D.; Xie, F.; Ashwehmbom, L.; Zhang, Z.; Tang, Q. Calibration of discrete element parameters and experimental verification for modelling subsurface soils. *Biosyst. Eng.* **2021**, *212*, 215–227. [CrossRef]
28. Kim, Y.S.; Lee, S.D.; Baek, S.M.; Baek, S.Y.; Jeon, H.H.; Siddique, M.A.; Kim, Y.J.; Kim, W.S.; Sim, T.; Yi, S.M.; et al. Development of DEM-MBD coupling model for draft force prediction of agricultural tractor with plowing depth. *Comput. Electron. Agric.* **2022**, *202*, 107405. [CrossRef]